 CMES, vol.10, no.2, pp.153-170, 2005

Stick-Slip-Slap Interface Response Simulation: Formulation and Application of a General Joint/Interface Element

Yaxin Song [1], D. Michael McFarland [1], Lawrence A. Bergman [1] and Alexander F. Vakakis [2]

Abstract: A general interface element is developed for dynamic response analysis of structures with jointed interfaces, which can account for damping due to both impact and friction. Contact effects are included through a segment-to-segment contact model which considers the stick-slip-slap behavior at every point along the joint interface. A nonlinear friction law is adopted at the interface to describe microscopic relative motion due to the deformation of the asperities on the interface. Numerical examples demonstrate that the general joint interface element is capable of accounting for both friction and impact damping in jointed interfaces, as well as capturing the transfer of vibrational energy from low frequency to high during impact. The development of an interface slip zone is a combined result of the actual friction traction and pressure distribution along the interfaces. It is shown that the general joint interface element is able to address this effectively, and the segment-to-segment contact model adopted here allows the general interface element to capture very detailed stick-slip behavior along the interfaces even with a coarse mesh.

keyword: Joint, Friction, Interface, Finite element, Contact model.

1 Introduction

Joint mechanics refers to the mechanical properties of joints in multi-component systems and their impact on the structural response of the system of which they are a part [Segalman, Paez, Smallwood, Sumali and Urbina (2003)]. The successful modeling of joints largely depends on understanding their basic physics and the ability to accurately predict their behavior. The nonlinear behavior and energy dissipation associated with mechanical joints are derived from two mechanisms: friction and impact (slap/gapping) [Segalman, Paez, Smallwood, Sumali and Urbina (2003); Folkman, Ferney, Bingham and Dutson (1996)]. Friction-related joint properties result from micro- and macro-slip occurring along the joint interface. The micro/macro-slip causes energy dissipation and change of interface stiffness, resulting in the nonlinear hysteresis associated with mechanical joints [Gaul and Lenz (1997)]. Impact occurs when two parts of an interface, which are originally separated by some finite gap, come into contact. Two mechanisms of energy dissipation are associated with impact. One is the small plastic deformation occurring in the zone of contact during the collision process, resulting in impact damping [Khulief and Shabana (1987); Lankarani and Nikravesh (1990)], and the other is the transfer of vibrational energy from low frequency to high where it is dissipated rapidly by material and friction damping mechanisms [Segalman, Paez, Smallwood, Sumali and Urbina (2003); Folkman, Ferney, Bingham and Dutson (1996); Onoda, Sano and Minesugi (1993)].

Considerable modeling effort has been expended attempting to quantify the nonlinear behavior of mechanical joints in structures containing them. Among these are the detailed finite element joint models that require solving a contact problem which incorporates a particular friction law. These are versatile and simple in concept [Lobitz, Gregory and Smallwood (2001); Segalman (2001)]. However, to capture micro-stick-slip-slap behavior, an extremely fine mesh must be used at the joint interfaces, which makes finite element joint models computationally prohibitive for dynamic analysis of jointed structures. A major difficulty arising in joint modeling research is the multi-scale problem. The constitutive behavior of mechanical joints, which appears as nonlinear damping, nonlinear stiffness, and a transfer of mechanical energy from low frequency to high, largely stems from micro-scale (say, 1 $\sim$ several hundred microns) in-

[1] Department of Aerospace Engineering, University of Illinois at Urbana-Champaign, Urbana, IL 61801, USA

[2] Department of Mechanical and Industrial Engineering and Department of Aerospace Engineering, University of Illinois at Urbana-Champaign, Urbana, IL 61801, USA. Division of Mechanics, National Technical University of Athens, GR-157 10 Zografos, Athens, Greece

terfacial interactions generally of interest to tribologists. On the other hand, the prediction of structural response of multi-component systems, which are significantly affected by those manifestations associated with the constitutive behavior of the joint, belongs to the area of structural dynamics and is associated with length scales of the overall structures (say, $1 \sim$ several dozen meters).

To circumvent the multi-scale difficulty, many researchers turn to reduced-order whole-joint models that can capture the overall effects of the joint on the dynamics of the structure, instead of developing models that exactly describe the micro-scale constitutive behavior of the joint itself. At this stage, major efforts in joints modeling focus on addressing friction-related joint behavior. Some researchers studied the effects of joints using a nonparametric joint model [Crawley and Aubert (1986); Crawley and O'Donnell (1987); Wang and Sas (1990); Ren and Beards (1998); Ren, Lim and Lim (1998); Liu and Ewins (2000)]. Other represented the friction occurring at contact interfaces by a single Coulomb friction model [Menq and Griffin (1985); Shaw (1986); Ferri and Heck (1998)], which is capable only of describing either the full-slip or full-stick situation. Different reduced-order models that allow partial slip on the friction interface were presented by Menq, Bielak and Griffin (1986); Menq, Griffin and Bielak (1986); Haessig and Friedland (1990); Canudas de Wit, Olsson, Åström and Lischinsky (1995); and Segalman (2001, 2002) to simulate the one-dimensional hysteretic behavior of joints. Song, Hartwigsen, Bergman and Vakakis (2003) and Song, Hartwigsen, McFarland, Bergman and Vakakis (2004) developed the 2-D/3-D adjusted Iwan beam element (AIBE) to represent joint behavior in two and three dimensional beam structures. Good agreement between simulated and experimental results showed that the AIBE can capture the transient response of jointed structures. However, as joints are often inseparable parts of structures with complex configurations, reduced-order whole-joint models are somewhat limited in application. Moreover, a common problem in whole-joint models is their inability to describe the transient relation between the varying normal pressure and tangential traction.

Impact-related behavior in joints is complicated and remains an area of continuing interest [Gronet, Pinson, Voqui, Crawley and Everman (1987); Crawley (1988)], and much effort has been devoted to general contact-impact problems. Some have investigated vibro-impact

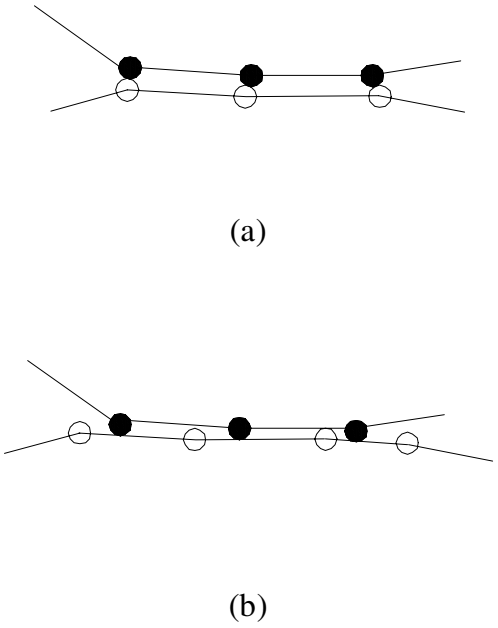

Figure 1 : Contact models. (a) Node-to-node contact model, (b) Node-to-segment contact model

phenomena in dynamic systems, in which impacts occur at discrete locations in flexible structures or collisions occur between rigid bodies [Cone and Zadoks (1995); Emaci, Nayfeh and Vakakis (1997); Knudsen and Massih (2000)]. Others have used finite element methods to examine more general contact-impact problems in continua. As mentioned earlier, finite element methods developed for general contact-impact problems have been employed directly to simulate the dynamics of joints with friction. In those analyses, node-to-node or node-to-segment contact models (NNC or NSC) are used, and contact is represented at discrete nodes, as shown in Fig. 1 [Zhong (1993)]. Therefore, an extremely fine mesh must be used along the joint interfaces to capture the micro-stick-slip behavior. Also, in conventional contact FE analysis, impact damping is generally neglected.

A general joint interface element incorporating both dynamic impact and friction is developed in this paper. Here, segment-to-segment contact (SSC) is considered, and contact effects are accounted for along continuous edges of the elements. Thus, stick-slip-slap behavior at every point along the joint interfaces is considered. In the segment-to-segment contact model, segment pairs are

specified in advance of the analysis, and contact is assumed to occur only between those segment pairs. This is generally true in dynamic analysis of jointed structures, since only small displacements and micro- and macro-slip occur at the joint interface. The general joint interface element is comprised of two parts: the joint impact element which accounts for impact effects (including impact damping) normal to the direction of the interface, and the joint friction element which considers friction along the interface. The joint impact element consists of a contact unit and a separation unit. The contact unit describes the impact between two points on the joint interface and will be active if the two points come into contact; the separation unit prevents two points on the interface from separating and is active when the two points separate beyond an initial clearance. In the joint friction element, a nonlinear friction law by Oden and Pires (1983) is adopted to describe the micro- and macro-slip phenomena along the interface.

Two numerical examples are given to illustrate the application of the general joint interface element. In the first example, a system of two cantilever beams under a concentrated impulse loading is considered, and the simulated results show that the general joint interface element is capable of accounting for the impact and friction damping in the joint, as well as capturing the transformation of vibration energy from low frequency to high due to impact. In the second example quasi-static and dynamic analyses of a contact system in which an elastic plate is pressed against a rigid base with a constant pressure and pulled laterally are presented. The two analyses demonstrate that the development of the interface slip zone is a combined result of the actual friction traction and pressure distributions along the interface, and the general joint interface element is able to address this effectively. It is shown that the segment-to-segment contact model allows the general interface element to describe very detailed stick-slip behavior along the interfaces even with a coarse mesh.

2 Finite Element Procedures for Elastodynamic Contact Problems

2.1 Overview

General contact problems are inherently nonlinear even for cases involving small displacements and the simplest constitutive relations because the contact area is unknown *a priori* and the boundary conditions are determined as part of the solution. Furthermore, for contact problems considering friction, unknown friction directions and modes (sticking, sliding) also contribute nonlinearities [Zhong (1993); Zhong and Mackerle (1994); Saleeb, Chen and Chang (1994); Farahani, Mofid and Vafai (2000)]. In the standard displacement-based finite element analysis of contact problems, displacements are constrained by the kinematic contact constraint or impenetrability condition; i.e., no material particle of one body is allowed to penetrate to the interior of another body. Two constraint methods are commonly used to enforce the impenetrability condition: the Lagrange multiplier method and the penalty method. In the Lagrange multiplier method [Hughes, Taylor, Sackman, Curnier and Kanoknukulchai (1976); Chaudhary and Bathe (1986); Bathe (1982); Cook, Malkus and Plesha (1989)], the contact forces (Lagrange multipliers) are calculated as unknowns, and the zero-penetration condition is enforced exactly. The Lagrange method increases the dimension of the resulting system equations and is not consistent with explicit integration procedures [Carpenter, Taylor and Katona (1991)]. In the penalty method [Zhong (1993); Bathe (1982); Cook, Malkus and Plesha (1989); Hunek (1993)], a small amount of penetration is allowed at contact points, and the contact force is assumed to be proportional to the amount of penetration by introducing a penalty parameter (or normal contact stiffness). The penalty method does not introduce new unknowns into the system equations, and the application of the penalty method with explicit integration is straightforward. However, the accuracy of the solution depends on the choice of penalty parameters.

The penalty method is equivalent to a "gap" or "joint" element method [Endo, Oden, Becker and Miller (1984); Simons and Bergan (1986); Choi and Chung (1996); Ju and Rowlands (1999)]. A gap element has nodes across the gap and its nodal displacements are coupled by the gap element stiffness matrix. When the gap is open (separation occurs) the element stiffness is set to zero, and when the gap is closed (contact occurs) the element stiffness is set to the normal contact stiffness.

In the above constraint methods, contact points must be determined first. A simple way of doing this is to specify node pairs prior to solution of the problem and to check these node pairs during the analysis to see whether they contact or not. This so called node-to-node inter-

face model is valid only for problems with small displacements, in which the deformed configuration does not deviate much from the initial configuration. For contact problems with large displacements or sliding, a contact-searching algorithm, the master-slave algorithm first presented by Hallquist (1978), is most widely used. The master-slave algorithm is a node-to-segment interface model.

2.2 Finite Element Procedures

We consider here deformable bodies $\Omega \subset \mathrm{R}^N$ (N=2 for two-dimensional problems; N=3 for three-dimensional problems), which have the boundary

$$\Gamma = \Gamma_d \cup \Gamma_f \cup \Gamma_c \tag{1}$$

where Γ_d is the portion of the boundary subjected to prescribed displacements; Γ_f is the portion of the boundary subjected to applied tractions; and Γ_c is the contact boundary between deformable bodies. Γ_d, Γ_f and Γ_c are mutually disjoint.

Let displacement, velocity and acceleration fields in domain Ω be $\mathbf{u}$, $\dot{\mathbf{u}}$ and $\ddot{\mathbf{u}} \in \mathrm{R}^N$, respectively. The governing equations for the elastodynamic contact problem include dynamic equilibrium equations (with kinematic and constitutive relations), boundary conditions, initial conditions, a friction law and contact conditions [Tamma, Li and Sha (1994); Sha, Tamma and Li (1996)]. Specifically, for a time interval $[0,T]$ the contact conditions are

$$g_n(\mathbf{x},\mathbf{u}) \geq 0 \quad \text{on } \Gamma_c \times [0,T] \tag{2a}$$

$$\sigma_n \leq 0 \quad \text{on } \Gamma_c \times [0,T] \tag{2b}$$

$$\sigma_n g_n(\mathbf{x},\mathbf{u}) = 0 \quad \text{on } \Gamma_c \times [0,T] \tag{2c}$$

in which $\mathbf{x} \in \mathrm{R}^N$ is the coordinate vector of a material point, g_n is the "gap" function between two bodies on the contact boundary Γ_c, and σ_n is the normal contact stress on Γ_c. Condition (2a) describes the impenetrability condition; (2b) implies that no tensile contact stress can occur on Γ_c; and (2c) is the complementary condition.

The elastodynamic contact problem stated above can be discretized and solved by finite element techniques. The equilibrium equation is first transformed into a variational equation by the application of the principle of virtual work

$$\begin{aligned}&\int_\Omega \rho \ddot{u}_i \delta u_i d\Omega + \int_\Omega c\dot{u}_i \delta u_i d\Omega + \int_\Omega \sigma_{ij}\delta\varepsilon_{ij} d\Omega \\ &= \int_\Omega b_i \delta u_i d\Omega + \int_{\Gamma_f} p_i \delta u_i d\Gamma + \int_{\Gamma_c} q_i \delta u_i d\Gamma\end{aligned} \tag{3}$$

where σ and ε are stress and strain tensors, respectively; ρ is the mass density; c is the linear viscous damping parameter which represents the system material damping; $\mathbf{b} \in \mathrm{R}^N$ is the body force; $\mathbf{p} \in \mathrm{R}^N$ denotes the surface traction on Γ_f; and $\mathbf{q} \in \mathrm{R}^N$ is the contact traction on Γ_c, which is constrained by contact conditions and friction laws. In the standard procedure, the domain Ω is discretized into a collection of finite elements. We denote the domain occupied by an element as Ω^e and its displacement, traction and contact boundaries as Γ_d^e, Γ_f^e and Γ_c^e, respectively. Within Ω^e, the displacement, velocity, acceleration, strain and stress fields can be expressed as

$$\mathbf{u} = \mathbf{N}\mathbf{d}^e, \quad \dot{\mathbf{u}} = \mathbf{N}\dot{\mathbf{d}}^e, \quad \ddot{\mathbf{u}} = \mathbf{N}\ddot{\mathbf{d}}^e \tag{4a}$$

$$\varepsilon = \mathbf{B}\mathbf{d}^e, \quad \sigma = \mathbf{D}\varepsilon = \mathbf{D}\mathbf{B}\mathbf{d}^e \tag{4b}$$

in which $\mathbf{d}^e$, $\dot{\mathbf{d}}^e$, and $\ddot{\mathbf{d}}^e$ are element displacement, velocity and acceleration vectors, respectively; $\mathbf{N}$ is the shape function matrix; and $\mathbf{B}$ and $\mathbf{D}$ are the strain-displacement and stress-strain matrices of the material, respectively. Substituting (4) into (3), we obtain the discrete finite element equations of motion for elastodynamic contact problems

$$\begin{aligned}&\left(\sum_e \int_{\Omega^e} \rho \mathbf{N}^T\mathbf{N} d\Omega\right)\ddot{\mathbf{d}} + \left(\sum_e \int_{\Omega^e} c\mathbf{N}^T\mathbf{N} d\Omega\right)\dot{\mathbf{d}} \\ &+ \left(\sum_e \int_{\Omega^e} \mathbf{B}^T\mathbf{D}\mathbf{B} d\Omega\right)\mathbf{d} \\ &= \sum_e \int_{\Omega^e} \mathbf{N}^T\mathbf{b} d\Omega + \sum_e \int_{\Gamma_f^e} \mathbf{N}^T\mathbf{p} d\Gamma + \sum_e \int_{\Gamma_c^e} \mathbf{N}^T\mathbf{q} d\Gamma\end{aligned} \tag{5}$$

which can be expressed as

$$\mathbf{M}\ddot{\mathbf{d}} + \mathbf{C}\dot{\mathbf{d}} + \mathbf{K}\mathbf{d} = \mathbf{F}_{ext} + \mathbf{F}_c \tag{6}$$

Here, $\mathbf{M}$, $\mathbf{C}$ and $\mathbf{K}$ are the system mass, viscous damping (associated with system material damping) and stiffness

matrices; $\mathbf{d}$, $\dot{\mathbf{d}}$ and $\ddot{\mathbf{d}}$ are the system displacement, velocity and acceleration vectors; $\mathbf{F}_{\text{ext}}$ is the external force vector, including body and surface forces; and $\mathbf{F}_c$ is the contact force vector.

As mentioned in Section 2.1, in addition to the usual initial and boundary conditions, displacement vector $\mathbf{d}$ in (6) is subjected to the impenetrability condition. The Lagrange multiplier method or the penalty method can be used to enforce the impenetrability condition, and the "gap" element method is equivalent to the penalty method. By introducing interface elements at joint interfaces, the impenetrability condition is satisfied, albeit approximately in the case of the penalty method. The contact force vector Γ_c is evaluated according to the contact force model and friction law adopted in the gap elements.

3 A Joint Interface Element without Friction

3.1 Description of the Joint Impact Interface Element

A two-dimensional joint interface element without friction is shown in Fig. 2. The joint interface element is placed between two adjoining edges of elements E_1 and E_2, which are used to discretize bodies 1 and 2, respectively. Elements E_1 and E_2 could be any element type, but here we use bilinear isoparametric elements with four nodes. The interface element of Fig. 2 is composed of an infinite number of interface units. Each interface unit has a contact unit, with initial clearance $e_I(s)$, and a separation unit, with initial clearance $e_S(s)$, where s is the local tangential coordinate along the edge of the interface element. Each separation unit is composed of a linear elastic spring with distribution stiffness $k_S(s)$. The form of the contact unit depends on the contact force model adopted. For example, a linear contact unit consists of a linear elastic spring and a viscous damper, as shown in Fig. 2. The contact unit will be active if two points on the joint interface come into contact, and the separation unit will be active when two points on the joint interface separate beyond the initial clearance $e_S(s)$. In Fig. 2, $F_1^n(s)$, $F_2^n(s)$ are the normal interface distribution force functions and $U_1^n(s)$, $U_2^n(s)$ are the normal displacements at point $s$on edges 1 and 2, respectively. A gap function $g_n(s)$ on the interface is defined as

$$g_n(s) = U_2^n(s) - U_1^n(s) - e_I(s) \tag{7}$$

Within a bilinear isoparametric element, displacements

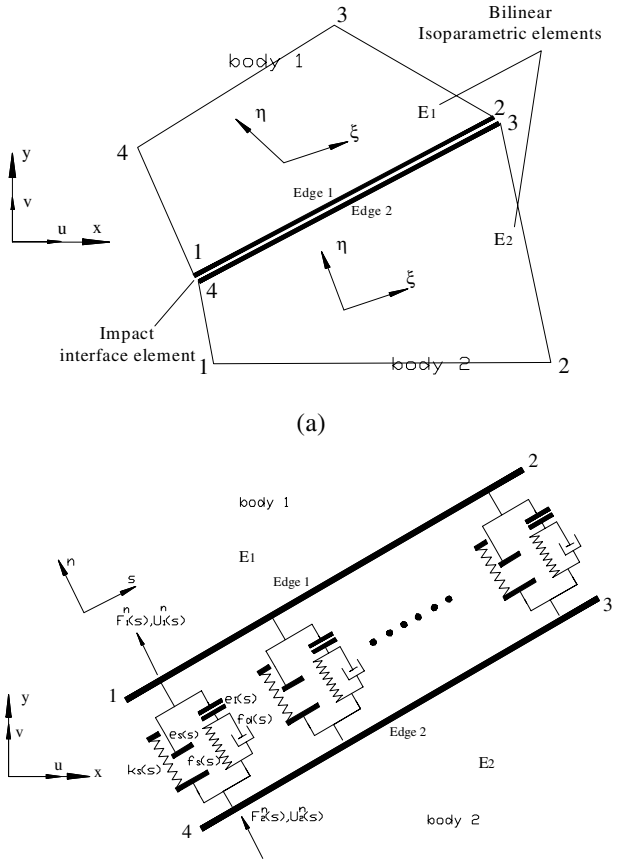

Figure 2 : Impact interface element for mechanical joints

at a point are interpolated as

$$\mathbf{u} = \mathbf{N}\mathbf{d}^e \tag{8a}$$

$$\mathbf{u} = \left\{ \begin{array}{cc} u & v \end{array} \right\}^T \tag{8b}$$

$$\mathbf{d}^e = \left\{ \begin{array}{cccccccc} u_1 & v_1 & u_2 & v_2 & u_3 & v_3 & u_4 & v_4 \end{array} \right\}^T \tag{8c}$$

$$\mathbf{N} = \left[\begin{array}{cccccccc} N_1 & 0 & N_2 & 0 & N_3 & 0 & N_4 & 0 \\ 0 & N_1 & 0 & N_2 & 0 & N_3 & 0 & N_4 \end{array} \right] \tag{8d}$$

where $N_i(\xi,\eta)$ $(i = 1,2,3,4)$ is the shape function. Coordinates within the element are defined by

$$x = \sum_{i=1}^{4} N_i x_i, \quad y = \sum_{i=1}^{4} N_i y_i \tag{9}$$

where (x_i, y_i) are the coordinates of node i, $i = 1,2,3,4$. In Fig. 2, at edge 1 ($\eta = -1$) and edge 2 ($\eta = +1$), we can evaluate $U_1^n(s)$ and $U_2^n(s)$ as

$$U_1^n(s) = \frac{\mathbf{R}_1}{l}\mathbf{N}_1\mathbf{d}_1^e \tag{10a}$$

$$U_2^n(s) = \frac{\mathbf{R}_2}{l}\mathbf{N}_2\mathbf{d}_2^e \tag{10b}$$

where

$$\mathbf{N}_1 = \left[\begin{array}{cccc} N_1 & 0 & N_2 & 0 \\ 0 & N_1 & 0 & N_2 \end{array}\right]_{\eta=-1} \tag{11a}$$

$$\mathbf{N}_2 = \left[\begin{array}{cccc} N_3 & 0 & N_4 & 0 \\ 0 & N_3 & 0 & N_4 \end{array}\right]_{\eta=+1} \tag{11b}$$

$$\mathbf{R}_1 = \left[\begin{array}{cc} -\frac{\partial y}{\partial \xi} & \frac{\partial x}{\partial \xi} \end{array}\right]_{\eta=-1}, \quad \mathbf{R}_2 = \left[\begin{array}{cc} -\frac{\partial y}{\partial \xi} & \frac{\partial x}{\partial \xi} \end{array}\right]_{\eta=+1} \tag{11c}$$

$$\begin{aligned} l &= 1/2\sqrt{(x_2-x_1)^2+(y_2-y_1)^2} \\ &= 1/2\sqrt{(x_4-x_3)^2+(y_4-y_3)^2} \end{aligned} \tag{11d}$$

$$\mathbf{d}_1^e = \left\{\begin{array}{cccc} u_1 & v_1 & u_2 & v_2 \end{array}\right\}_{E1}^T,$$

$$\mathbf{d}_2^e = \left\{\begin{array}{cccc} u_3 & v_3 & u_4 & v_4 \end{array}\right\}_{E2}^T \tag{11e}$$

Here, in the expressions for $\mathbf{d}_1^e$ and $\mathbf{d}_2^e$, the subscripts "E1" and "E2" denote from which element the displacements are obtained. The gap function $g_n(s)$ can be expressed as

$$g_n(s) = \frac{1}{l}\mathbf{P}\mathbf{d}_I^e - e_I(s) \tag{12}$$

Obviously,

$$\mathbf{P} = \left[\begin{array}{cc} -\mathbf{R_1}\mathbf{N_1} & \mathbf{R_2}\mathbf{N_2} \end{array}\right], \quad \mathbf{d}_I^e = \left\{\begin{array}{cc} \mathbf{d}_1^e & \mathbf{d}_2^e \end{array}\right\}^T \tag{13}$$

where $\mathbf{d}_I^e$ is the nodal displacement vector for the impact interface element, which has four nodes numbered clockwise as shown in Fig. 2(b).

The interface distribution forces at point s are

$$\begin{aligned} F_1^n(s) &= -F_2^n(s) \\ &= \alpha(s) f_I(s) + \beta(s) k_S(s)\left[g_n(s) + e_S(s) + e_I(s)\right] \end{aligned} \tag{14}$$

in which the impact force $f_I(s) = f_s(s) + f_d(s)$, where $f_s(s)$ and $f_d(s)$ are elastic and damping distribution forces in the contact unit, respectively, and

$$\alpha(s) = \left\{\begin{array}{ll} 1, & if \quad g_n(s) > 0 \\ 0, & If \quad g_n(s) \le 0 \end{array}\right. \tag{15a}$$

$$\beta(s) = \left\{\begin{array}{ll} 1, & \text{if} \quad g_n(s) + e_S(s) + e_I(s) \le 0 \\ 0, & \text{else} \end{array}\right. \tag{15b}$$

The element nodal force vector for the joint impact interface element due to contact-impact, $\mathbf{f}_I^e$, can be calculated from the interface force distribution functions $F_1^n(s)$ and $F_2^n(s)$ in the form

$$\begin{aligned} \mathbf{f}_I^e &= \left\{\begin{array}{cccccccc} f_{x1} & f_{y1} & f_{x2} & f_{y2} & f_{x3} & f_{y3} & f_{x4} & f_{y4} \end{array}\right\}^T \\ &= \left\{\begin{array}{c} \int\limits_{S_{c1}} \mathbf{N}_1^T F_1^n ds \\ \int\limits_{S_{c2}} \mathbf{N}_2^T F_2^n ds \end{array}\right\} \\ &= \left\{\begin{array}{c} \int\limits_{-1}^{1} \mathbf{N}_1^T F_1^n \left\{\begin{array}{c} -\partial y/\partial \xi \\ \partial x/\partial \xi \end{array}\right\}_{\eta=-1} d\xi \\ \int\limits_{-1}^{1} \mathbf{N}_2^T (-F_2^n) \left\{\begin{array}{c} \partial y/\partial \xi \\ -\partial x/\partial \xi \end{array}\right\}_{\eta=+1} d\xi \end{array}\right\} \\ &= -\int_{-1}^{1} \left[\begin{array}{c} -\mathbf{N}_1^T \mathbf{R}_1^T \\ \mathbf{N}_2^T \mathbf{R}_1^T \end{array}\right] F_1^n d\xi \\ &= -\int_{-1}^{1} \mathbf{P}^T F_1^n d\xi \end{aligned} \tag{16}$$

where f_{xi} and f_{yi} (i =1,2,3,4) represent the nodal forces in the x and y directions for the ith node of the impact interface element, and S_{c1} and S_{c2} are edges 1 and 2, respectively.

Assembling the element nodal force vectors for all joint impact interface elements, we obtain the contact force vector for the system as

$$\mathbf{F}_c = \sum_e \mathbf{f}_I^e \tag{17}$$

In this joint impact interface element, the impact force within the contact unit is the sum of elastic force $f_s(s)$ and damping force $f_d(s)$, which are given according to the chosen contact force models. Generally, $f_s(s)$ is a function of $g_n(s)$ and $f_d(s)$ is a function of both $g_n(s)$ and $\dot{g}_n(s)$. Therefore, the contact force vector is a function of displacement, velocity and clearance. Assuming that $e_I(s)$ and $e_S(s)$ are known, the system equation of motion (6) becomes

$$\mathbf{M}\ddot{\mathbf{d}} + \mathbf{C}\dot{\mathbf{d}} + \mathbf{K}\mathbf{d} = \mathbf{F}_{\text{ext}} + \mathbf{F}_c(\mathbf{d}, \dot{\mathbf{d}}) \tag{18}$$

3.2 Joint Interface Element with Linear Contact Force Model

Many different contact force models have been developed (see, for example, [Khulief and Shabana (1987); Lankarani and Nikravesh (1990); Hunt and Crossley (1975); Khulief and Shabana (1986)]). In the contact unit introduced in Section 3.1, if a linear contact force model is adopted

$$f_I(s) = f_s(s) + f_d(s) = k_I g_n(s) + c_I \dot{g}_n(s) \tag{19}$$

(in which k_I and c_I are the coefficients of elastic and damping distribution forces, respectively), the element damping and stiffness matrices of the joint impact interface element can be derived. Substitution of (19) and (12) into (14) leads to

$$\begin{aligned} F_1^n(s) &= -F_2^n(s) \\ &= [\alpha(s)k_I(s) + \beta(s)k_S(s)]\frac{\mathbf{P}}{l}\mathbf{d}_I^e + \alpha(s)c_I(s)\frac{\mathbf{P}}{l}\dot{\mathbf{d}}_I^e \\ &\quad + \beta(s)k_S(s)e_S(s) - \alpha(s)k_I(s)e_I(s) \end{aligned} \tag{20}$$

By substituting (20) into (16), the element nodal force vector for the joint impact interface element can be expressed as

$$\mathbf{f}_I^e = -\mathbf{K}_I^e \mathbf{d}_I^e - \mathbf{C}_I^e \dot{\mathbf{d}}_I^e + \mathbf{E}_I^e \tag{21}$$

where

$$\mathbf{K}_I^e = \frac{1}{l}\int_{-1}^{1} [\alpha k_I + \beta k_S]\,\mathbf{P}^T\mathbf{P}\,d\xi \tag{22a}$$

$$\mathbf{C}_I^e = \frac{1}{l}\int_{-1}^{1} \alpha c_I \mathbf{P}^T\mathbf{P}\,d\xi \tag{22b}$$

$$\mathbf{E}_I^e = \int_{-1}^{1} \mathbf{P}^T(\alpha k_I e_I - \beta k_S e_S)\,d\xi \tag{22c}$$

Here, $\mathbf{C}_I^e$ and $\mathbf{K}_I^e$ are the elemental damping and stiffness matrices, and $\mathbf{E}_I^e$ is the elemental nodal force vector due to clearance, for the impact interface element. Therefore, the system equation of motion in (18) has the form

$$\mathbf{M}\ddot{\mathbf{d}} + (\mathbf{C} + \mathbf{C}_I)\dot{\mathbf{d}} + (\mathbf{K} + \mathbf{K}_I)\mathbf{d} = \mathbf{F}_{\text{ext}} + \mathbf{E}_I \tag{23}$$

in which

$$\mathbf{C}_I = \sum_e^{\mathbf{C}_I^e}, \quad \mathbf{K}_I = \sum_e^{\mathbf{K}_I^e}, \quad \mathbf{E}_I = \sum_e^{\mathbf{E}_I^e} \tag{24}$$

4 A Joint Interface Element with Impact and Friction

4.1 General Joint Interface Element

The joint impact interface element given in Section 3 does not include frictional effects. A general joint interface element considering both impact and friction effects is presented in this section. This element is composed of two parts: one is the joint impact interface element given in Section 3, which accounts for impact in the normal direction of the interface, and the other is the joint friction interface element, which considers the friction along the interface. In both the impact and friction interface elements, segment-to-segment contact along edges of the elements is considered.

The general interface and friction interface elements have the same element nodal displacements as the impact interface element, given by

$$\begin{aligned} \mathbf{d}_{IF}^e = \mathbf{d}_I^e = \mathbf{d}_f^e &= \left\{ \begin{array}{cccccccc} u_1 & v_1 & u_2 & v_2 & u_3 & v_3 & u_4 & v_4 \end{array} \right\}^T \\ &= \left\{ \left\{ \begin{array}{cccc} u_1 & v_1 & u_2 & v_2 \end{array} \right\}_{E1} \left\{ \begin{array}{cccc} u_3 & v_3 & u_4 & v_4 \end{array} \right\}_{E2} \right\}^T \end{aligned} \tag{25a}$$

The element nodal force vector for the general interface element is composed of two parts

$$\begin{aligned} \mathbf{f}_c^e = \mathbf{f}_I^e + \mathbf{f}_f^e &= \left\{ \begin{array}{cccccccc} f_{x1} & f_{y1} & f_{x2} & f_{y2} & f_{x3} & f_{y3} & f_{x4} & f_{y4} \end{array} \right\}^T \end{aligned} \tag{25b}$$

where $\mathbf{f}_I^e$ (as shown in (16)) and $\mathbf{f}_f^e$ are element nodal force vectors due to impact and friction, respectively.

4.2 Joint Friction Interface Element Using a Nonlinear Friction Law

Although it has been widely used in engineering applications, the classical Coulomb friction law cannot describe the microscopic relative motion corresponding to the deformation of the asperities of two contacting bodies, which has been observed to occur even under a small tangential force. Therefore, we adopt a more complex nonlinear friction law by Oden and Pires (1983) for our joint friction interface element. In this law, the friction traction $\mathbf{f}_T$ has a relationship with the tangential relative displacement $\mathbf{u}_T$ as illustrated in Fig. 3, where a constant normal contact force f_n is assumed. For monotonically

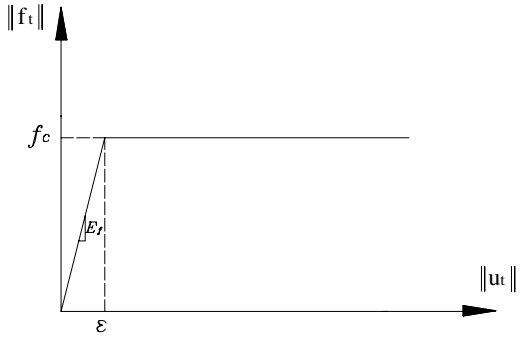

Figure 3 : Relation of friction force and relative tangential displacement in the nonlinear friction law for initial loading

increasing loading (in a positive or negative sense), we have

$$\mathbf{f}_T = \begin{cases} -E_f \mathbf{u}_T, & \text{if} \quad \|\mathbf{u}_T\| \le \varepsilon \\ -f_c \mathbf{u}_T / \|\mathbf{u}_T\|, & \text{if} \quad \|\mathbf{u}_T\| > \varepsilon \end{cases} \tag{26}$$

in which $f_c = \mu |f_n|$ where μ is the coefficient of friction and $\varepsilon = f_c/E_f$. The quantityE_f, referred to as the friction modulus, is the slope of the curve before macro-slip.

Fig. 4 shows the joint friction interface element using the nonlinear friction law, in which the normal contact force distribution functions $F_1^n(s)$ and $F_2^n(s)$ account only for compressive traction; that is,

$$F_1^n(s) = -F_2^n(s) = \alpha(s) f_I(s) \tag{27}$$

(this may be compared to (14)). The relative displacement function at point s on the interface is calculated as

$$\begin{aligned} U_t(s) = {} & (u_1 N_1 + u_2 N_2)\cos\theta + (v_1 N_1 + v_2 N_2)\sin\theta \\ & - (u_3 N_3 + u_4 N_4)\cos\theta - (v_3 N_3 + v_4 N_4)\sin\theta \end{aligned} \tag{28}$$

With the knowledge of $F_1^n(s)$, $F_2^n(s)$ and $U_t(s)$, the friction tractions $F_1^s(s)$ and $F_2^s(s)$ can be determined through the nonlinear friction law. The element nodal force vector for the joint friction interface element, $\mathbf{f}_f^e$, is obtained

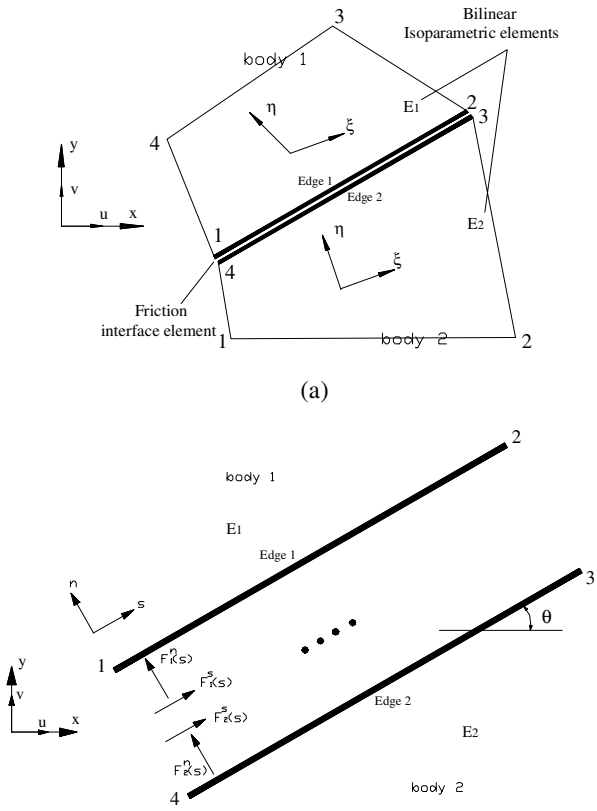

Figure 4 : Joint friction interface element using nonlinear friction law

as (refer to (25b))

$$\begin{aligned} \mathbf{f}_f^e &= \begin{Bmatrix} \int_{S_{c1}} \mathbf{N}_1^T F_1^s(s) ds \\ \int_{S_{c2}} \mathbf{N}_2^T F_2^s(s) ds \end{Bmatrix} \\ &= \begin{Bmatrix} \int_{-1}^{1} \mathbf{N}_1^T F_1^s \begin{Bmatrix} \partial x/\partial\xi \\ \partial y/\partial\xi \end{Bmatrix}_{\eta=-1} d\xi \\ \int_{-1}^{1} \mathbf{N}_2^T (-F_1^s) \begin{Bmatrix} \partial x/\partial\xi \\ \partial y/\partial\xi \end{Bmatrix}_{\eta=+1} d\xi \end{Bmatrix} \end{aligned} \tag{29}$$

5 Applications to Contact Problems

5.1 Numerical Example I: A System of Two Cantilever Beams

A system of two cantilever beams under a concentrated impulsive load at the mid-span of the upper beam, as shown in Fig. 5(a), is considered. The finite element

Table 1 : Four dynamic simulation cases for the two-cantilever-beam system of Example I

	Impact damping?	Friction?	Separation?
Case I	×	×	√
Case II	√	×	√
Case III	×	×	×
Case IV	×	√	×

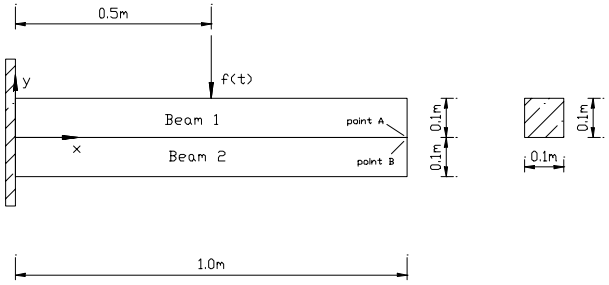

(a)

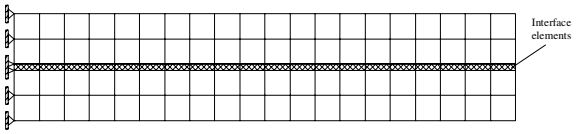

(b)

Figure 5 : Two cantilever beams under a concentrated load. (a) Configuration, (b) Finite element mesh

mesh for this system is shown in Fig. 5(b). The interface between the two beams is represented by 20 general joint interface elements. The two beams are identical in geometry and material properties, except that they have different mass densities. The material properties for the two beams are Young's modulus E = 2.0×10^{11} N / m^1, Poisson's ratio ν = 0.0, and mass density ρ_1 = 4.0×10^3 kg / m^3 for beam 1, while ρ_2 = 7.8×10^3 kg/m^3 for beam 2. The load is the half-sine function

$$f(t)=\begin{cases} 1.0\times10^7\sin(2\pi f_{imp}t)\,\mathrm{N}, & 0\le t\le 1/(2f_{imp}) \\ 0, & \text{else} \end{cases} \tag{30}$$

where $f_{\mathrm{imp}} = 2000$ Hz. Four cases are simulated to demonstrate the application of the joint interface element and its potential in dynamic response prediction of structures containing joints/interfaces. As shown in Tab. 1, in Cases I and II the two beams can separate freely (the stiffness of the separation units is zero), and there is no friction in the interface. No impact damping is considered in case I, while it is accounted for in Case II. In Cases III and IV, the two beams are bonded so that they cannot separate freely, and in both cases these is no impact damping. The difference between Cases III and IV is that in Case IV there is friction at the interface, while there is none in Case III. The parameters of the interface elements in the four cases are given in Tab. 2. In all cases, the system material damping matrix $\mathbf{C}$in (6) is represented by Rayleigh damping in the form $\mathbf{C}=\overline{\alpha}\mathbf{M}+\overline{\beta}\mathbf{K}$ [Bathe (1982); Cook, Malkus and Plesha (1989)], where the coefficients $\overline{\alpha}$ and $\overline{\beta}$ were obtained by setting the first two damping ratios of the system to $\varsigma_1=\varsigma_2=0.005$.

Figures 6 through 9 show the acceleration histories in the x and y directions at points A and B for the four cases. In Figs. 6 (Case I) and 7 (Case II), the two beams impact at some times because they have different dynamic characteristics (the fundamental natural frequencies for beam 1 and 2 are 120.4 and 86.2 Hz, respectively). Comparing the responses in Figs. 6 and 7, it is clear that impact damping can have a significant effect on the dynamic response of a system with an interface. In Figs. 8 (Case III) and 9 (Case IV), the two beams are bonded together and vibrate like a single beam without impact occurring. Due to the damping resulting from frictional energy dissipation, the responses in Fig. 9 decay faster than those in Fig. 8, although the difference between them is not as obvious as that between Cases I and II.

In both Cases I and III, no friction or impact damping is considered. However, if we compare the response histories for Cases I (Fig. 6) and III (Fig. 8), it is obvious that the vibration of the two beams in Case I decays much more quickly than that in Case III. In Case I we have two separate beams which impact each other during vibration, while in Case III there is practically no impact occurring because the two beams are bonded together. As mentioned in Section 1, the interfacial energy dissipation stems from friction and impact (slapping). Further, the

Table 2 : Parameters of interface elements in four simulations of Example I

	$k_I(N/m)^2$	$c_I(Ns/m)^3$	$e_I(m)$	$k_S(N/m)^2$	$e_S(m)$	$E_f(N/m)^2$	μ
Case I	1.0×10^{11}	N/A	0.0	N/A	0.0	N/A	N/A
Case II	1.0×10^{11}	1.0×10^{7}	0.0	N/A	0.0	N/A	N/A
Case III	1.0×10^{11}	N/A	0.0	1.0×10^{11}	0.0	N/A	N/A
Case IV	1.0×10^{11}	N/A	0.0	1.0×10^{11}	0.0	1.0×10^{10}	0.4

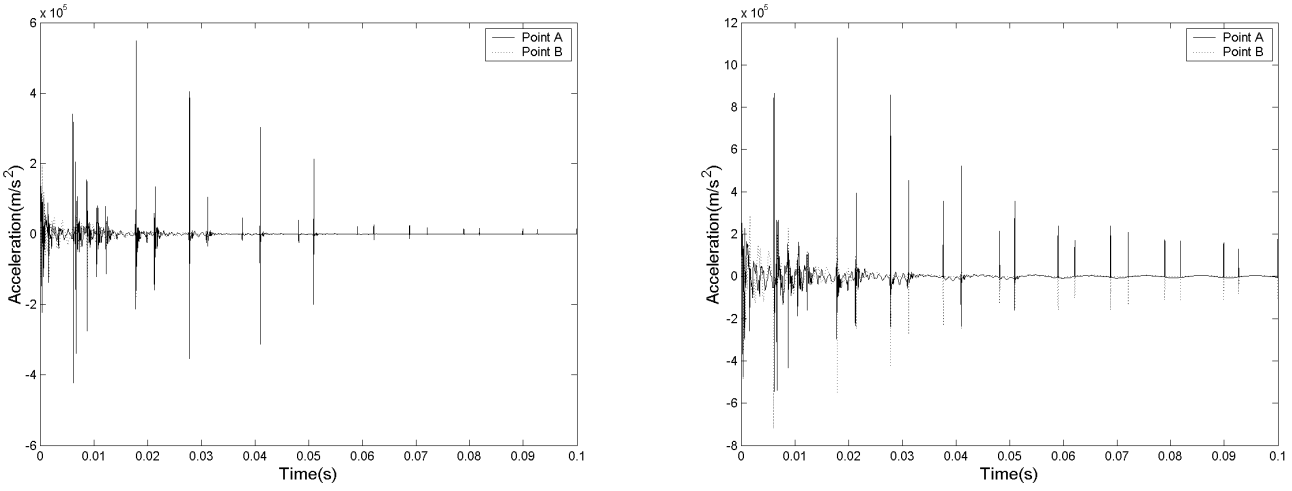

(a) (b)

Figure 6 : Acceleration histories for points A and B in Case I. (a) In the x-direction, (b) In the y-direction

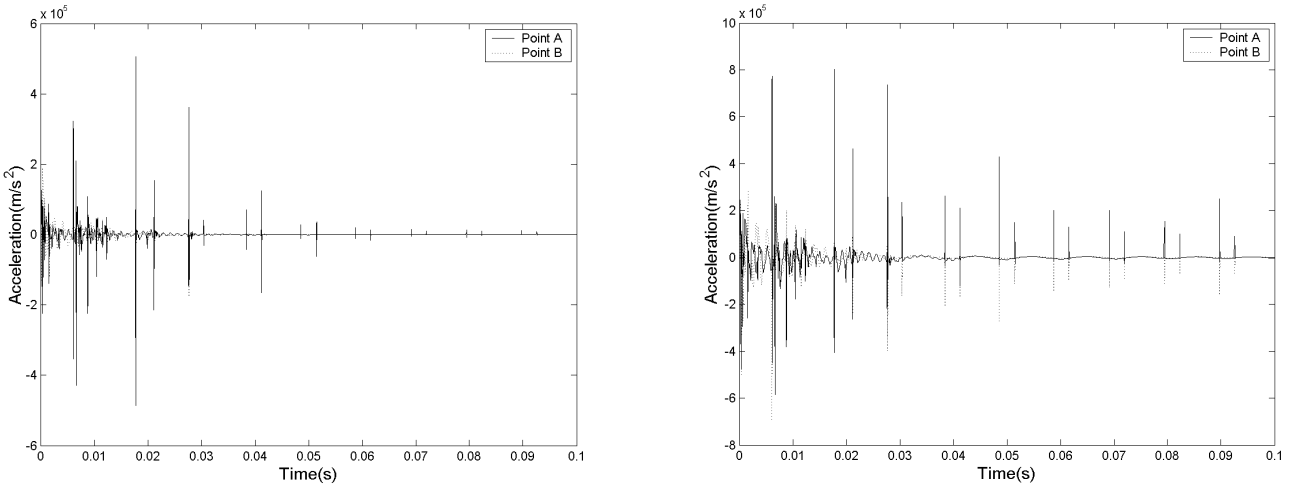

(a) (b)

Figure 7 : Acceleration histories for points A and B in Case II. (a) In the x-direction, (b) In the y-direction

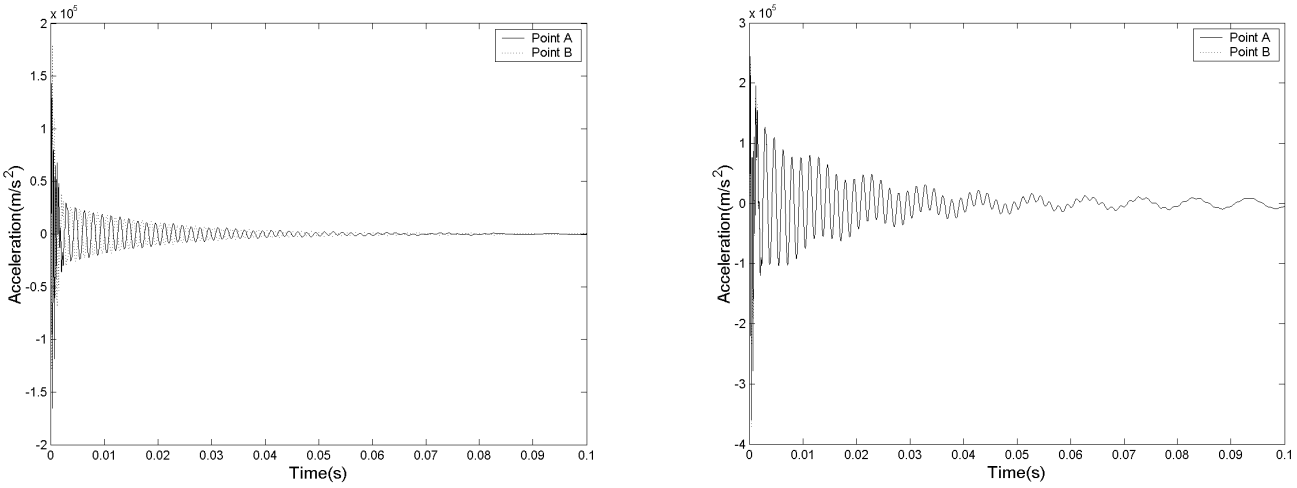

Figure 8 : Acceleration histories for points A and B in Case III. (a) In the x-direction, (b) In the y-direction

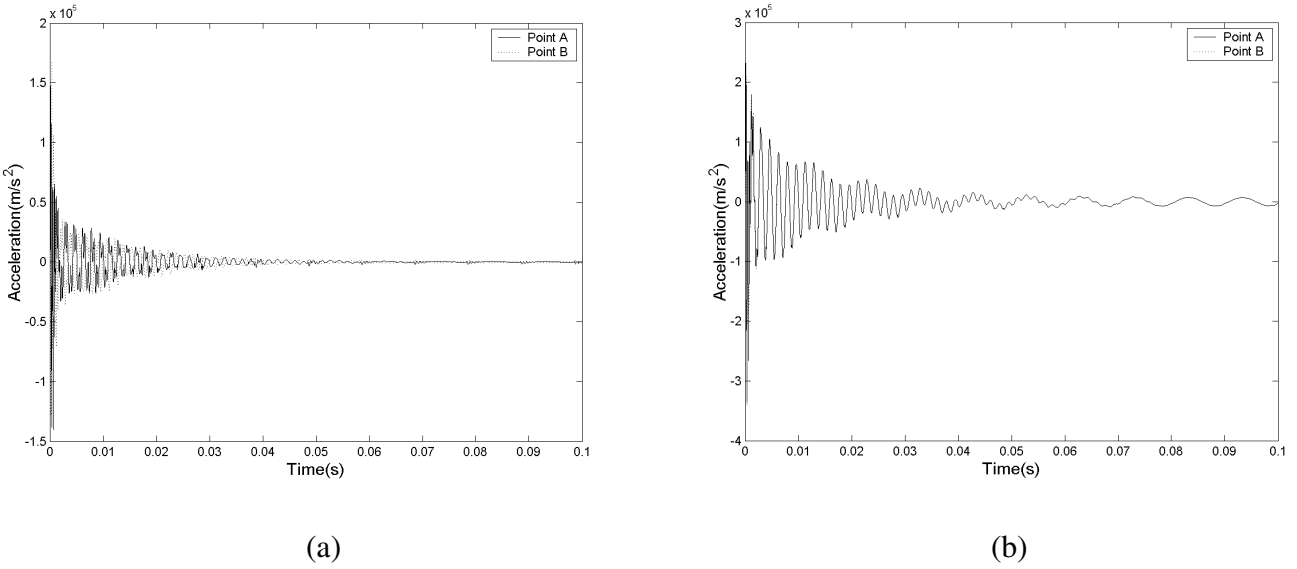

Figure 9 : Acceleration histories for points A and B in Case IV. (a) In the x-direction, (b) In the y-direction

energy dissipation associated with impact is due to two mechanisms: (a) small plastic deformation in the contact zone, which is accounted for in the interface element by the distributed dampers in the normal direction of the interface, and (b) the transformation of vibrational energy from low to high frequency where it is dissipated rapidly by material damping. The rapid decay of vibration in Case I is exactly due to the mechanism (b), which is shown clearly in Figs. 10 and 11. These figures show the magnitudes of the Fourier transforms of the acceleration histories for the four cases for points A and B, respectively. Comparing with Cases III and IV, the vibrational energy in Cases I and II is distributed over a wider range, to higher frequency, in the presence of impact. For Case IV, as shown in Figs. 10 and 11, there are some peaks excited by friction in the x direction. These peaks cor-

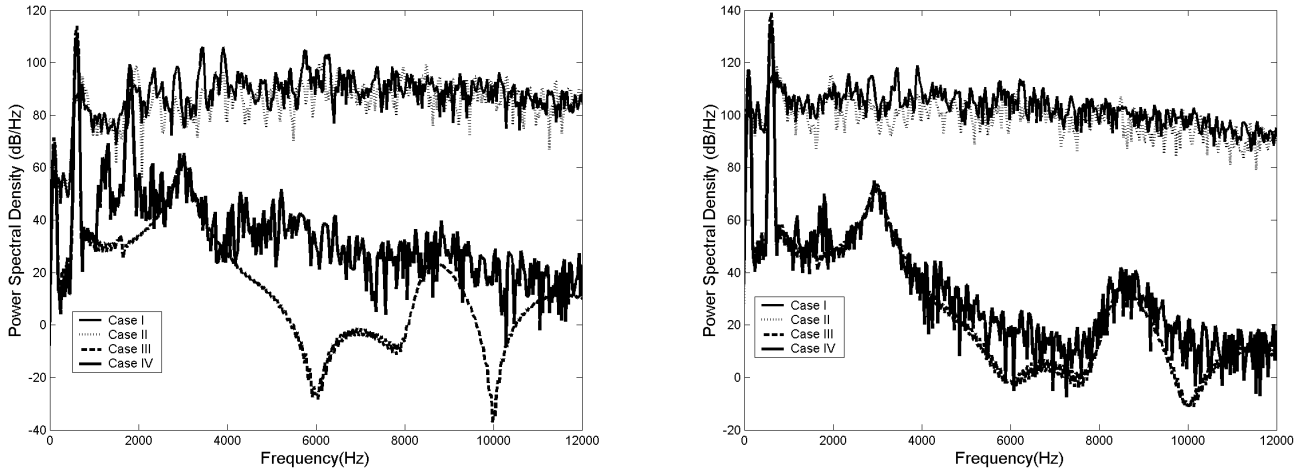

(a) (b)

Figure 10 : Magnitudes of the Fourier transforms of the acceleration histories for point A. (a) In the x-direction, (b) In the y-direction

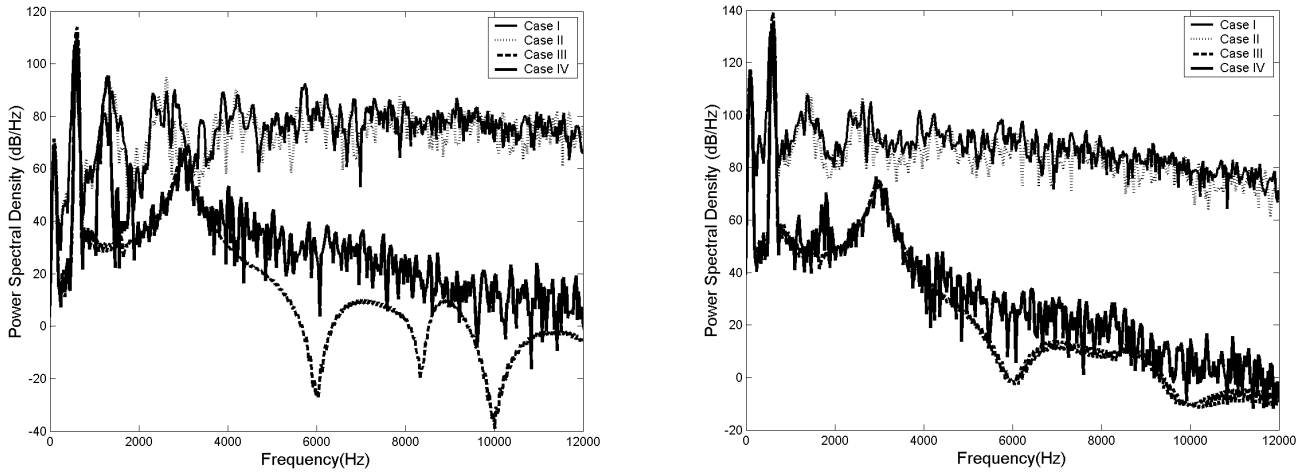

(a) (b)

Figure 11 : Magnitudes of the Fourier transforms of the acceleration histories for point B. (a) In the x-direction, (b) In the y-direction

respond to the first extensional modes of the upper and lower beams (around 1768 and 1266 Hz). Therefore, the presence of friction may also excite some high-frequency vibration; however, this is less significant than the energy transformation due to impact.

5.1.1 Preliminary Experimental Corroboration of Impact Behavior Predictions

The above results may be compared to experimental data taken with the apparatus of Fig. 12. The two impacting cantilevered beams shown there are nominally identical except for length, with one being 10% shorter than the

other. The measured transverse accelerations following impulsive excitation (with a modal testing hammer) are plotted in Fig. 13, where qualitative agreement with the above numerical findings is quite evident. Full-scale values in this plot represent accelerations of approximately 500 m/s^2, which is significantly less than the values obtained in the simulations; however, additional, unmodeled damping mechanisms, such as displacement of air from between the beams, were present in the experiment. Transformation of these signals to the frequency domain (not shown here) reveals that significant vibrational energy is shifted from low to high frequency by the impacts occurring early in the response.

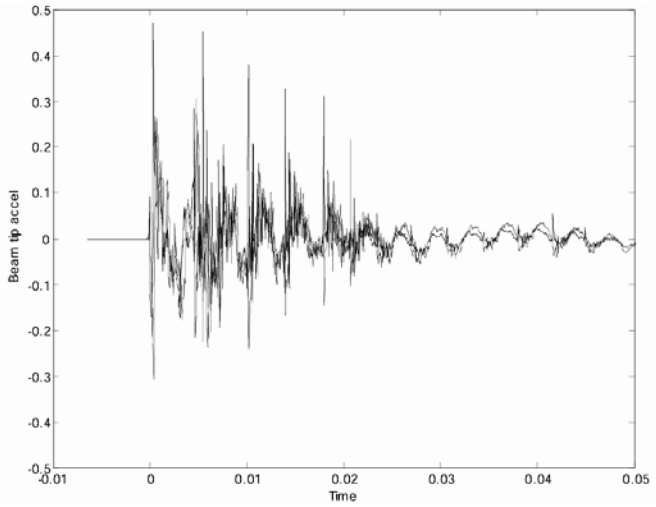

Figure 13 : Acceleration of beam tips following impulse (hammer) excitation; spikes correspond to impact (slapping) of the beams

5.2 Numerical Example II: An Elastic Plate Pressed Against a Rigid Base

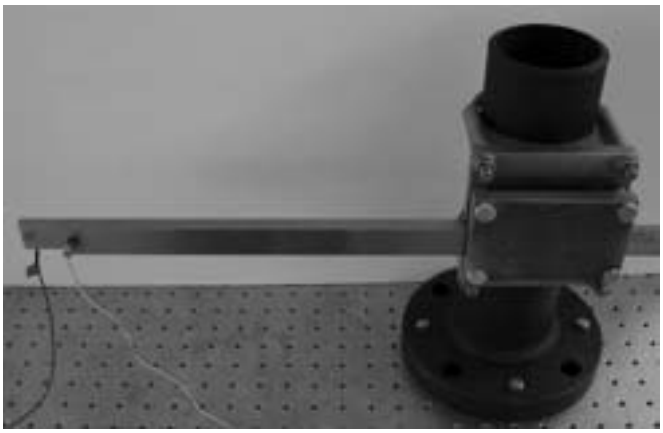

Figure 12 : Cantilevered beams, identical except for length, mounted in a bench-top clamping fixture

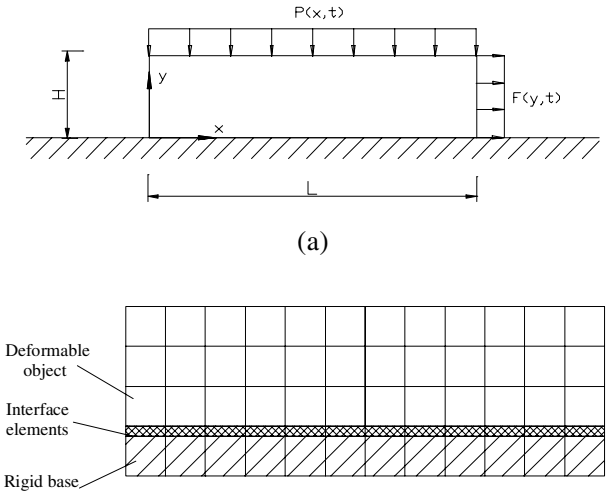

Figure 14 : An elastic plate pressed on a rigid base and pulled laterally. (a) Configuration, (b) Finite element mesh

Figure 14(a) shows a contact system in which an elastic plate is pressed against a rigid base with a pressure $P(x,t)$ and is pulled laterally at the right end of the plate by a force distribution $F(y,t)$. This system is modeled as a plane-strain problem. The material properties for the elastic plate are Young's modulus E = 2.0×10^{11} N / m^1, Poisson's ratio ν = 0.3, and mass density $\rho = 7.8\times10^3$ kg / m^3. The geometry of the plate is length $L = 0.36$ m, height $H = 0.09$ m, and width $W = 1.0$ m. The finite element mesh for this system is shown in Fig. 12(b). Twelve general joint interface elements are located at the interface of the elastic plate and the rigid base. The parameters of the interface elements used in the simulation are $k_I = 3.3\times10^{12}$ N/m^2, c_I = 0.0 Ns/m^3, $e_I = e_S = 0.0$ m, E_f =1.0×10^{10} N/m^2, and μ =0.4.

To carry out a quasi-static analysis for this system, the pressure $P(x,t)$and the pulling force distribution $F(y,t)$ shown in Fig. 15 were applied, in which $P(x,t) = 1.0\times10^4$ N/m and $F_{\max} = \alpha_F F_{\lim}/H$, where $F_{\lim} = \mu PL$ is the critical friction force and α_F is the loading fac-

tor. In this quasi-static simulation, $\alpha_F = 1.0$, $t_1 = 0.02$ s, and $t_2 = 0.04$ s. No friction is considered when $t \le t_1$. The system material damping matrix **C** is again represented by Rayleigh damping with very large damping ratios ($\varsigma_1 = \varsigma_2 = 0.95$) to help eliminate dynamic structural response.

Figures16(a) and (b) show the histories of the pressure and the friction state along the interface between the elastic plate and rigid base. Due to the clockwise couple caused by the pulling force, the pressure near the right end of the interface is larger than the constant pressure P, while the pressure near the left end is smaller. The pressure around the center of the interface maintains a value close to P (see Fig. 16(a)). This specific pressure distribution has a direct effect on the development of the slip zone along the interface. As shown in

Fig. 16(b) (a value of 1 represents sliding and a value of 0 means non-sliding), the slip starts from the left end of the interface and extends gradually to the right as the pulling force increases. This is quite different from the corresponding one-dimensional problem, where the pressure is constant all along the interface and the slip zone begins and extends from the right-hand end of the interface to the left.

A dynamic simulation was performed next. In the dynamic analysis, everything is the same as in the quasi-static analysis except that the force distribution $F(y,t)$ is a harmonic function

$$F(y,t) = \begin{cases} 0, & 0 \le t < t_1 \\ \alpha_F \frac{F_{\lim}}{H} \sin[1000\pi(t-t_1)], & \text{else} \end{cases} \tag{31}$$

where $\alpha_F = 0.6$ and $t_1 = 0.02$s. In this simulation, the material damping matrix **C** is again in the form of Rayleigh damping. When $t \le t_1$, no friction is considered and the Rayleigh damping coefficients $\overline{\alpha}$ and $\overline{\beta}$ are determined by two very large damping ratios ($\varsigma_1 = \varsigma_2 = 0.95$), while for $t > t_1$, another Rayleigh damping matrix with the first two damping ratios set to $\varsigma_1 = \varsigma_2 = 0.005$ was used.

Figures 17(a) and (b) show the histories of the pressure and the friction state at the interface, respectively. During the simulation, the pressure distribution at the interface is changing all the time with the harmonic force function $F(y,t)$. Basically, as $F(y,t)$ increases in the positive x direction (the plate is "pulled" to the right), the pressure near the right end of the interface (referred to as P_2)

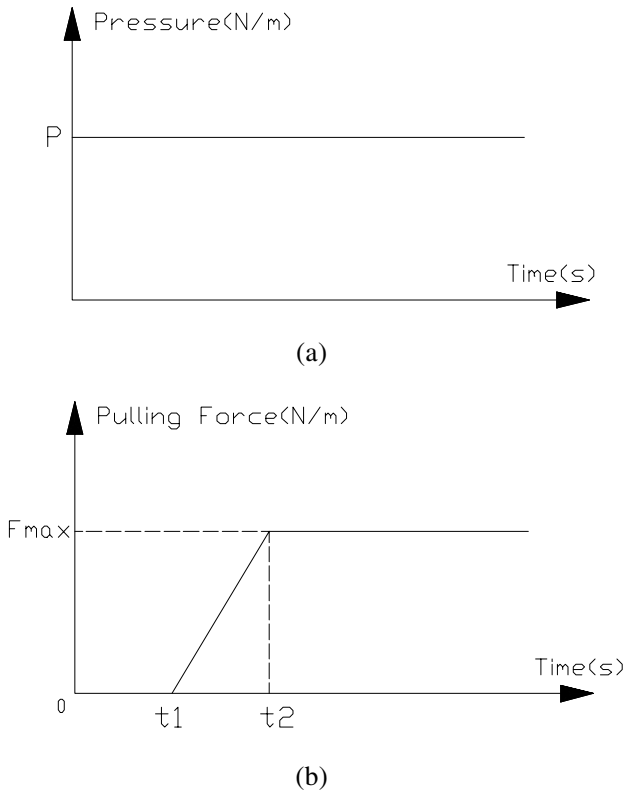

Figure 15 : Pressure and pulling force functions for the contact system. (a) Pressure, (b) Pulling force

increases to a value larger than the constant pressure P, while the pressure near the left end of the interface (referred to as P_1) decreases to a value smaller than P. As $F(y,t)$ increases in the negative x direction (the plate is "pushed" to the left), the change in pressure distribution is the opposite, i.e., P_1 increases to a value larger than P and P_2 decreases to a value smaller than P. During the "pulling" and "pushing" processes, the pressure around the center of the interface is changing and has a value between P_1 and P_2. These effects of "pulling" and "pushing" loadings on interface pressure distribution have also been observed by Heinstein and Segalman (2002). Along with the dynamic effects on the structural response, this changing pressure distribution at the interface causes a very complicated friction state, as shown in Fig. 17(b).

In the above quasi-static and dynamic simulations, for each interface element, sixteen Gauss points along the edge of the element were employed in evaluating the element nodal force vector due to friction (two-point Gauss quadrature was used, and each interface element edge

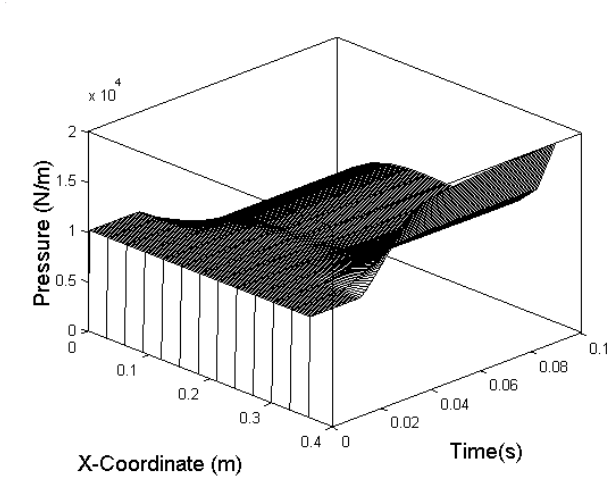

(a)

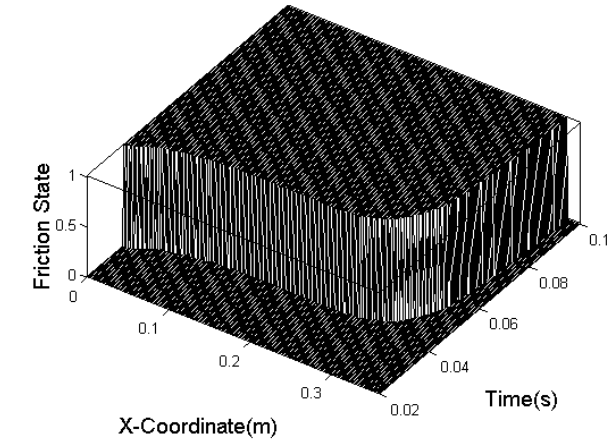

(b)

Figure 16 : Quasi-static simulation results. (a) Pressure distribution, (b) Friction state

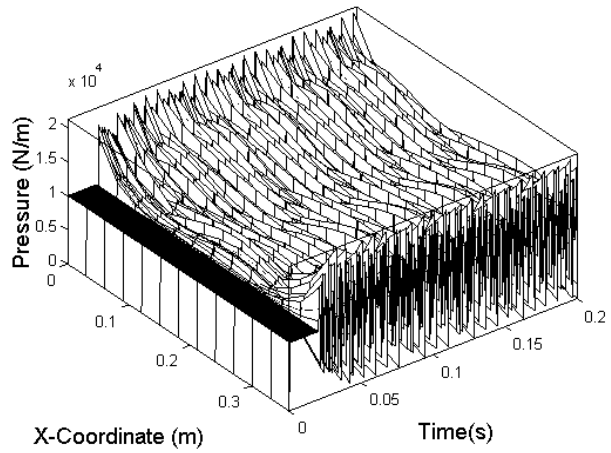

(a)

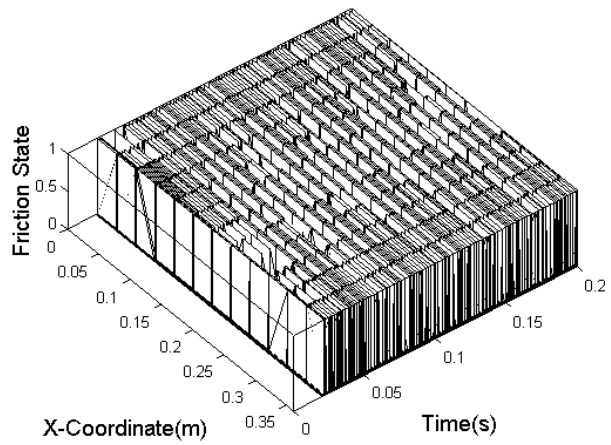

(b)

Figure 17 : Dynamic simulation results. (a) Pressure distribution, (b) Friction state

was divided into 8 parts). It can be seen from Figs. 16(b) and 17(b) that very detailed stick-slip behavior along the interface can be captured even with a coarse mesh.

6 Conclusion

Joint modeling research is hindered by the dramatically different length scales associated with joint properties and the length scale characteristic of the overall structures. In conventional finite element joint models, node-to-node or node-to-segment contact models are employed, and the contact effects are accounted for at discrete nodes. To capture the micro-stick-slip behavior along joint interfaces, an extremely fine mesh must be used. Also, in conventional contact finite element analysis, impact damping due to small plastic deformation in the contact zone is generally neglected. Some researchers have developed reduced-order whole-joint models that can capture the overall effects of joints on dynamics of jointed structures to overcome the multi-scale difficulty in joint modeling research. However, these reduced-order whole-joint models usually are not versatile enough to model arbitrary structural configurations and are incapable of describing the transient relation between the varying normal pressure and tangential traction.

The authors have developed a general joint interface el-

ement incorporating both dynamic impact and friction, in which segment-to-segment contact is considered and contact effects are accounted for continuously along the edges of the elements. Thus, stick-slip behavior at every point along the joint interfaces is considered even when using a relatively coarse mesh. The general interface element is applicable to structure geometries and configurations and it is easy to incorporate any dynamic friction and contact model into it. Numerical examples demonstrate that the general joint interface element is capable of capturing all nonlinear joint properties due to interface impact and friction.

The successful application of this element in dynamic response analysis of jointed structures hinges on the determination of the interface parameters associated with the dynamic contact and friction laws adopted. It is never an easy job to choose the appropriate penalty parameter (or normal contact stiffness), damping parameter, friction modulus (or tangential contact stiffness), and so on. A promising methodology to overcome this is to find ways to link the parameters of the joint interface element with physical interfacial quantities as represented by an asperity-based model developed in tribology.

Acknowledgement: This work was partially supported by Sandia National Laboratories through Contracts Number DOE SNL BF-0162 and DOE SNL 267009, and by the Office of Naval Research through Contract Number N00014-00-1-10187. The authors are grateful to Dr. Daniel Segalman for generously sharing his insights into this problem.

Personal thoughts Those of us who knew Cliff, particularly as new faculty trying to find our way at NSF, certainly remember his kind and supportive attitude. He was quick to offer advice and always patient. Throughout the years, it was a pleasure to drop in on him. The ensuing conversations were always long and enjoyable, ranging over many topics. We miss him.

References

Bathe, K. J. (1982): *Finite Element Procedures in Engineering Analysis*. Prentice-Hall, Inc.

Canudas de Wit, C.; Olsson, H.; Åström, K. J.; Lischinsky, P. (1995): A new model for control of system with friction. IEEE *Transactions on Automatic Control*, vol. 40, no. 3, pp. 419-425.

Carpenter, N. J.; Taylor, R. L.; Katona, M. G. (1991): Lagrange constraints for transient finite element surface contact. *International Journal for Numerical Methods in Engineering*, vol. 32, pp. 103-128.

Chaudhary, A. B.; Bathe, K. J. (1986): a solution method for static and dynamic analysis of three-dimensional contact problems with friction. *Computers & Structures*, vol. 24, pp. 855-873.

Choi, C.-K.; Chung, G. T. (1996): A gap element for three-dimensional elasto-plastic contact problems. *Computers & Structures*, vol. 61, no. 6, pp. 1155-1167.

Cone, K. M.; Zadoks, R. I. (1995): A numerical study of an impact oscillator with the addition of dry friction. *Journal of Sound and Vibration*, vol. 188, no. 5, pp. 659-683.

Cook, R. D.; Malkus, D. S.; Plesha, M. E. (1989): *Concepts and Applications of Finite Element Analysis*, third edition, John Wiley & Sons, Inc.

Crawley, E. F.; Aubert, A. C. (1986): Identification of nonlinear structural elements by force-state mapping," *AIAA Journal*, vol. 24, no. 1, pp. 155-162.

Crawley, E. F.; et al. (1988): Prediction and measurement of damping in hybrid scaled space structure models. Report SSL 7-88, Space System Laboratory, Department of Aeronautical and Astronautical Engineering, Massachusetts Institute of Technology.

Crawley, E. F.; O'Donnell, K. J. (1987): Force-state mapping identification of nonlinear joints," *AIAA Journal*, vol. 25, pp. 1003-1010.

Emaci, E.; Nayfeh, T.; Vakakis, A. F. (1997): Numerical and experimental study of nonlinear localization in a flexible structures with vibro-impacts. *Z. angew. Math. Mech*. vol. **77**, no. 7, pp. 527-541.

Endo, T.; Oden, J. T.; Becker, E. B.; Miller, T. (1984): A numerical analysis of contact and limit-point behavior in a class of problems of finite elastic deformation. *Computers & Structures*, vol. 18, no. 5, pp. 899-910.

Farahani, K.; Mofid, M.; Vafai, A. (2000): A solution method for general contact-impact problems. *Computational Methods in Applied Mechanics and Engineering*, vol. 187, pp. 69-77.

Ferri, A. A.; Heck, B. S. (1998): Vibration analysis of dry friction damped turbine blades using singular perturbation theory. *ASME Journal of Vibration and Acoustics*, vol. 120, pp. 588-595.

Folkman, S.; Ferney, B.; Bingham, J.; Dutson, J. (1996): Friction and impact damping in a truss using pinned joints. In: A. Guran, F. Pfeiffer and K. Popp, eds., *Dynamics with Friction: Modeling, Analysis and Experiment, Part I*, Series on Stability, Vibration and Control of Systems, Series B, no. **7**, pp. 137-168.

Gaul, L.; Lenz, J. (1997): Nonlinear dynamics of structures assembled by bolted joints," *Acta Mechanica*, vol. 125, pp. 169-181.

Gronet, M. J.; Pinson, E. D.; Voqui, H. L.; Crawley, E. F.; Everman, M. R. (1987): Preliminary design analysis and costing of a dynamic scale model of the NASA space station. NASA Contractor Report 4068, pp. 13-31.

Haessig, D. A.; Friedland, B. (1990): On the modeling and simulation of friction. *ASME Journal of Dynamic Systems, Measurement, and Control*, vol. 113, pp. 354-362.

Hallquist, J. O. (1978): A numerical treatment of sliding interfaces and impact. In: *Computer Technology for Interface Problems*, ASME Applied Mechanics Division, Winter Annual Meeting, vol. 30, pp. 117-133.

Heinstein, M. W.; Segalman, D. J. (2002): Bending effects in the frictional energy dissipation in lap joints. Report SAND2002-0083, Sandia National Laboratories, Albuquerque, NM.

Hughes, T. J. R.; Taylor, R. L.; Sackman, J. L.; Curnier, A.; Kanoknukulchai, W. (1976): A finite element method for a class of contact-impact problems. *Computational Methods in Applied Mechanics and Engineering*, vol. 8, pp. 249-276.

Hunek, I. (1993): On a penalty formulation for contact-impact problems. *Computers & Structures*, vol. 48, no. 2, pp. 193-203.

Hunt, K. H.; Crossley, F. R. E. (1975): Coefficient of restitution interpreted as damping in vibroimpact. *ASME Journal of Applied Mechanics*, vol. 42, pp. 440-445.

Ju, S. H.; Rowlands, R. E. (1999): A three-dimensional frictional contact element whose stiffness matrix is symmetric. *ASME Journal of Applied Mechanics*, vol. 66, pp. 460-467.

Khulief, Y. A.; Shabana, A. A. (1986): Dynamic analysis of constrained system of rigid and flexible bodies with intermittent motion. *ASME Journal of Mechanisms, Transmissions, and Automation in Design*, vol. 108, pp. 38-45.

Khulief, Y. A.; Shabana, A. A. (1987): A continuous force model for the impact analysis of flexible multibody systems. *Mech. Mach. Theory*, vol. 22, no. 3, pp. 213-224.

Knudsen, J.; Massih, A. R. (2000): Vibro-impact dynamics of a periodically forced beam. *ASME Journal of Pressure Vessel Technology*, vol. 122, pp. 210-221.

Lankarani, H. M.; Nikravesh, P. E. (1990): A contact force model with hysteresis damping for impact analysis of multibody systems. *Journal of Mechanical Design*, vol. 112, pp. 369-376.

Liu, W.; Ewins, D. J. (2000): Substructure synthesis via elastic media Part I: Joint identification. In: Proceedings of the 18^{th} International Modal Analysis Conference, pp. 1153-1159, San Antonio.

Lobitz, D. L.; Gregory, D. L.; Smallwood, D. O. (2001): Comparison of finite element predictions to measurements from the Sandia microslip experiment. In: Proceedings of 19^{th} International Modal Analysis Conference, Kissimmee, FL.

Menq, C.-H.; Bielak, J.; Griffin, J. H. (1986): The influence of microslip on vibratory response, Part I: A new microslip model. *Journal of Sound and Vibration*, vol. 107, no. 2, pp. 279-293.

Menq, C.-H.; Griffin, J. H. (1985): A comparison of transient and steady state finite element analysis of the forced response of a frictionally damped beam," *ASME Journal of Vibration, Acoustics, Stress, and Reliability in Design*, vol. 107, pp. 19-25.

Menq, C.-H.; Griffin, J. H.; Bielak, J. (1986): The influence of microslip on vibratory response, Part II: A comparison with experimental results. *Journal of Sound and Vibration*, vol. 107, no. 2, pp. 295-307.

Oden, J. T.; Pires, E. B. (1983): Nonlocal and nonlinear friction laws and variational principles for contact problems in elasticity. *Journal of Applied Mechanics*, vol. 50, pp. 67-76.

Onoda, J.; Sano, T.; Minesugi, K. (1993): Passive vibration suppression of truss by using backlash," Paper Number AIAA-93-1549-CP, In: 34^{th} AIAA/ASME/ASCE/AHS/ASC Structures, Structural Dynamics and Materials Conferences, La Jolla, CA, April 19-22.

Ren, Y.; Beards, C. F. (1998): Identification of 'effective' linear joints using coupling and joint identification

techniques. *ASME Journal of Vibration and Acoustics*, vol. 120, pp. 331-338.

Ren, Y.; Lim, T. M.; Lim, M. K. (1998): Identification of properties of nonlinear joints using dynamic test data. *ASME Journal of Vibration and Acoustics*, vol. 120, pp. 324-330.

Saleeb, A. F.; Chen, K.; Chang, T. Y. (1994): An effective two-dimensional frictional contact model for arbitrary curved geometry. *International Journal for Numerical Methods in Engineering*, vol. 37, pp. 1297-1321.

Segalman, D. J. (2001): An initial overview of Iwan modeling for mechanical joints. Report SAND2001-0811, Sandia National Laboratories, Albuquerque, NM.

Segalman, D. J. (2002): A four-parameter Iwan model for lap-type joints. Report SAND2002-3828, Sandia National Laboratories, Albuquerque, NM.

Segalman, D. J.; Paez, T.; Smallwood, D.; Sumali, A.; Urbina, A. (2003): Status and integrated road-map for joints modeling research," Report SAND2003-0897, Sandia National Laboratories, Albuquerque, NM.

Sha, D.; Tamma, K. K.; Li, M. (1996): Robust explicit computational developments and solution strategies for impact problems involving friction. *International Journal for Numerical Methods in Engineering*, vol. 39, pp. 721-739.

Shaw, S. W. (1986): On the dynamic response of a system with dry friction. *Journal of Sound and Vibration*, vol. 108, no. 2, pp. 305-325.

Simons, J. W.; Bergan, P. G. (1986): A finite element formulation of three-dimensional contact problems with slip and friction. *Computational Mechanics*, vol. 1, pp. 153-164.

Song, Y.; Hartwigsen, C. J.; Bergman, L. A.; Vakakis, A. F. (2003): A three-dimensional nonlinear reduced-order predictive joint model. *Journal of Earthquake Engineering and Engineering Vibration*, vol. 2, no. 1, pp. 59-74.

Song, Y.; Hartwigsen, C. J.; McFarland, D. M.; Bergman, L. A.; Vakakis, A. F. (2004): Simulation of dynamics of beam structures with bolted joints using adjusted Iwan beam elements. *Journal of Sound and Vibration*, vol. 273, nos. 1–2, pp. 249–276.

Tamma, K. K.; Li M.; Sha, D. (1994): Conjugate gradient based projection: a new explicit computational methodology for frictional contact problems. *Communications in Numerical Methods in Engineering*, vol. 10, pp. 633-648.

Wang, J.; Sas, P. (1990): A method for identifying parameters of mechanical joints," *ASME Journal of Applied Mechanics*, vol. 57, pp. 337-342.

Zhong, Z-H (1993): *Finite Element Procedures for Contact-Impact Problems*. Oxford University Press Inc., New York.

Zhong, Z-H; Mackerle, J. (1994): Contact-impact problems: a review with bibliography. *Applied Mechanics Reviews*, vol. 47, no. 2, pp. 55-76.